RSC Advances

ROYAL SOCIETY OF CHEMISTRY

www.rsc.org/advances

1   **Preparation of sponge-like biocomposite agarose-chitosan scaffold with**

2   **primary hepatocytes for establishing an in-vitro 3D liver tissue model**

3   **Anuj Tripathi and Jose Savio Melo***

4   Nuclear Agriculture and Biotechnology Division, Bhabha Atomic Research Centre, Mumbai -

5   400 085, India

6   Authors E-mail: anujtri@barc.gov.in and jsmelo@barc.gov.in

7   *Fax: +91-22-25505151; Tel: +91-22-25592760

8

9

10

11

12

13

14

15

16

17

18

19

20

21

22

23

24

25   **Abstract**

26   Designing a three-dimensional (3D) macroporous scaffold with desired bio-functional properties

27   is an important aspect for fabricating in vitro liver tissue model with applications in pre-clinical

28   therapeutics testing. In the present study a bio-polymeric composite scaffold of agarose-chitosan

29   (AG-CH) was synthesized at optimized sub-zero temperature and evaluated for its suitability in

30   the in-vitro liver tissue engineering. The scaffold showed high porosity (83 ± 2 %) with

31   interconnected pores (average pore diameter 40-70 µm). High swelling kinetics on account of the

32   hydrophilic pore channels in AG-CH scaffold allows unhindered migration of cells and gaseous

33   exchange. At neutral pH, the negative charge on the surface of AG-CH scaffold ensures

34   increased cell-to-cell interfacial interaction followed by colonization of hepatocytes. Rheological

35   studies of the hydrated scaffold demonstrates its high sponge-like visco-elastic behavior without

36   any fracture deformation upto 34 ± 1 N, which insinuates its applicability for soft-tissue

37   engineering. AG-CH scaffold showed ~ 15% degradation in a span of four weeks in sterile PBS

38   at physiological pH, which could help to maintain the structural integrity of neo-tissue formation.

39   *In-vitro* primary hepatocytes proliferation in AG-CH scaffold showed an increase in cellular

40   metabolic activity. The hepatic functions like albumin secretion and urea synthesis were

41   established for the primary hepatocytes in the 3D scaffold and were higher in comparison to the

42   control. The expression of hepatic CYP450 biomarker was observed in the in-vitro cultured

43   hepatocytes immobilized in 3D AG-CH scaffold. Thus, AG-CH scaffold with suitable physico-

44   chemical properties and hepatic cell compatibility present its potential for developing an in-vitro

45   liver tissue model.

46

47

1. Introduction

48

49 The gold standard for evaluating toxicological profile of therapeutic agents involves complex in-

50 vivo testing, Moreover, use of animals, cost, time constraints and ever increasing number of

51 therapeutics that need to be tested, is the major concern in the in-vivo testing of drugs. Therefore,

52 establishing the in-vitro 3D culture systems has become a priority for the toxicologist.[1] The use

53 of in-vitro tissue models have several advantages like decrease in animal numbers, the reduced

54 cost for their maintenance, the less time for drug testing, requirement for small quantity of

55 chemicals and also increase in throughput screening of multiple samples and their metabolites.[1,2]

56 In recent past, various in-vitro liver tissue models have been developed using liver-derived

57 components like liver tissue slices, immortalized liver cells, perfused liver and also primary

58 hepatocytes.[1] Among others, primary hepatocytes and immortalized cell lines are most widely

59 used in the in-vitro liver tissue models. However, loss of cell viability and decreases in liver

60 specific functions are the shortcoming of these models. Thus, recent developments are focused

61 towards the in-vitro engineering of 3D liver tissue and bio-artificial liver.[3] Liver tissue

62 engineering has emerged as a potential therapeutic approach to overcome these limitations for

63 hepatotoxicity analysis and can replace or enhance the current standard practice of organ

64 transplantation.[3,4] Porous scaffold integrated with liver cells can recreate biological tissue

65 substitutes with structural and functional features of liver tissue.

66   Biomimetic scaffolds are a key component in 3D tissue engineering (TE) that balance cell

67 adhesion and proliferation, temporary mechanical properties with amiable mass transport, to aid

68 biological delivery and in-vitro tissue regeneration. Several design processes were studied for the

69 fabrication of 3D porous scaffolds, but were often found to be not adequate due to lack of control

70 on scaffold architecture, porosity, and cellular interactions.[5] More importantly, biocompatibility

71 of the scaffold is imperative and must not elicit cytotoxic responses. The scaffold should have

72 significant mechanical properties and should not disintegrate or deform during the application.[6]

73 Designing of a scaffold should also take into account the possibility for easy sterilization to

74 prevent it from infection.[7] A typical porosity of 80 to 90% with average pore diameter of at least

75 60-100 µm is required for cell penetration and vascularization of the ingrown tissue.[8,9] Afore

76 mentioned requirements for scaffold material are numerous. To fulfill as many requirements as

77 possible, several designing approaches have been proposed.[10] Today, foremost focus in

78 designing of tissue engineering scaffolds is towards the use of natural polymers due to their

79 inherent bioactive properties, which improve cellular interaction and proliferation.[11,12]

80 Interestingly, composites of natural polymers have shown increase in mechanical stability and

81 improved cell interaction.[13-15] In a recent study, a hydrogel synthesized using de-cellularized

82 liver ECM has also been proposed for liver tissue regeneration by encapsulating primary

83 hepatocytes.[16]

84 Among the several natural polymers, only a few like agarose and chitosan have the attractive

85 properties required for liver tissue engineering. Agarose hydrogels have been used for seeding of

86 hepatocytes and have shown enhanced production of extracellular matrix.[17] Agarose is also well

87 documented for its high mechanical strength, controlled degradation and ability to maintain the

88 cellular phenotype.[15,18,19] However, agarose alone is not suitable to mimic the microenvironment

89 for hepatocytes. Thus, incorporation of ECM-like component could facilitate biomimetic

90 properties in the porous 3D scaffold, Chitosan obtained by the deacetylation of chitin, shows

91 structural analogy to the important liver tissue component i.e. glycosaminoglycans (GAGs).[20]

92 Earlier studies reported that GAGs which is found in abundance in the extracellular matrix

93 (ECM) of liver cells, induces synthesis and expression of gap junctions in the tissue and regulate

94 intercellular communication in the liver.[21] Chitosan has been shown to have excellent

95 biocompatibility, biodegradability, non-toxicity, adsorption properties and ability to be degraded

96 by lysozyme, a naturally occurring enzyme in human body fluid.[22]

97 In the present study, we have attempted to synthesize an elastic and degradable 3-D polymeric

98 composite scaffold with interconnected macroporous architecture. The biopolymers agarose and

99 chitosan were used in different concentrations to optimize the scaffold characteristics. The

100 scaffold was characterized by physico-chemical and rheological techniques. Further, primary rat

101 hepatocytes were grown under *in-vitro* condition in the scaffold to examine the cell-material

102 interaction by morphological analysis. Cell viability and functionality were accessed to evaluate

103 the suitability of the scaffold for fabricating in-vitro 3D liver tissue models.

104 **2. Experimental**

105 **2.1. Materials**

106 Chitosan (MW: 50,000-190,000 Da; degree of deacetylation $\geq$ 75 % and viscosity: 20-300 cps),

107 Glutaraldehyde solution (25%), sodium cyanoborohydride (NaBH$_3$CN) (25%), Dulbecco's

108 modified Eagle's medium (DMEM), penicillin-streptomycin antibiotic, collagenase type I and 3-

109 (4,5-dimethylthiazol-2-yl)-2,5-diphenyltetrazolium bromide (MTT) ($\geq$97.5%) were purchased

110 from Sigma-Aldrich Chemie (Steinheim, Germany). Agarose (low EEO (-Mr): 0.09-0.13, gelling

111 strength: ~1200g cm^{-2}, gelling temperature: ~38–40 ºC) was purchased from Sisco Research

112 Laboratories (Mumbai, India). Dimethyl sulfoxide (DMSO) ($\geq$99%) was purchased from Merck

113 (Mumbai, India). Glacial acetic acid was bought from BDH (Leicestershire, UK). Primary

114 hepatocyte cells were gifted by Dr. D. Singh (Yeungnam University, South Korea). All other

115 chemicals were of analytical grade and used without further purification.

116   **2.2. Methods**

117   **2. 2.1. Preparation of agarose-chitosan (AG-CH) scaffolds**

118   Chitosan powder (MW: 50,000-190,000 Da; degree of deacetylation $\geq$ 75% and viscosity: 20-

119   300 cps) was dissolved in 1% aqueous acetic acid solution (pH ~ 2.5) with the help of a

120   mechanical stirrer at room temperature (final concentration; 0.5%, 1% and 1.5%; w/v). In

121   separate 50 ml plastic tube, agarose (low EEO, -Mr: 0.09-0.13, gelling strength: ~1200g cm^{-2},

122   gelling temperature: ~38–40 °C) (final concentration; 1%, 2%, 3%, 4% and 5%; w/v) was

123   dissolved in deionized water (dH$_2$O) by boiling until a clear transparent solution was obtained.

124   Chitosan solution was then added to agarose solution in different polymer ratios (Table 1). These

125   solutions were further cooled at room temperature till the solution temperature dropped to ~ 45

126   °C. Further, glutaraldehyde (80 µL of 25%, v/v dissolved in 420 µL of dH$_2$O) was mixed gently

127   to each polymer mixture, to a final concentration of 0.2% in 10 mL solution. Immediately the

128   polymer solution was poured into moulds (2 mL and 5 mL plastic syringes) and incubated at -12

129   °C for 16 h in a liquid cryo-bath. After the incubation, monoliths were thawed in dH$_2$O.

130   Thereafter, the monoliths were extensively washed with dH$_2$O followed by drying under vacuum

131   at -45 °C for 24 h (Martin Christ, Germany). These synthesized scaffolds were then stored in air-

132   tight tubes at room temperature for further studies.

133   **2.2.2. Physico-chemical characterization of scaffolds**

134   *A. Microstructure and porosity analysis*

135   Surface gold coating of scaffolds were performed at 20 mA for 3 min using an ion sputter coater

136   (Hoyeon Tech., Model- HC 21, South Korea) for studying the physical morphology of scaffolds

137   using scanning electron microscope (SEM, FEI Quanta 200). The microscope was operated

138   under high vacuum at 10 kV with a sample spot size of 3 to 5 mm. According to the Archimede's

139   principle, porosity of scaffold was theoretically calculated using the following equation.[23]

140         $Porosity = (M_W-M_D)/ (M_W-M_{SUB})$

141   where, M_W is the water saturated wet mass of the scaffold, M_D is the dry mass of the scaffold,

142   and M_{SUB} is the submerged mass of the scaffold.

143   *B. Swelling Kinetics and Swelling Ratio*

144   The swelling analysis of AG-CH scaffold (8 mm diameter and 3 mm height) was carried out in

145   phosphate buffer saline (PBS; pH 7.4) at room temperature (27 °C $\pm$ 2) till the scaffold reached

146   its equilibrium. The swelling kinetics (at regular time intervals) and swelling ratio (SR) were

147   calculated using the following equations;

148         $W_U = [(W_T - W_D)/ W_E] \times 100$

149         $S.R = (W_E - W_D) / W_D$

150   where, W_U is the water uptake capacity of the porous scaffold, S.R. is swelling ratio, W_T is the

151   wet weight of the scaffold at different time intervals, W_D is the dry weight of the scaffold, and

152   W_E is the wet weight of scaffold at swelling equilibrium.

153   *C. Hydraulic permeability analysis*

154   The hydraulic permeability of the polymeric monoliths was determined using Darcy's law which

155   describes relationship between the liquid flow rate and pressure. The AG-CH scaffold (8 mm

156   diameter, 5 mm height) was placed in the permeability measurement setup and a constant water

157   pressure head was applied on the porous scaffold for 2 min. The flushed water was then collected

158   from the outlet and weighed. For the control experiment, no scaffold was placed between the

159   flow-path. The hydraulic permeability was calculated by applying the recorded values to the

160   following equation.[23,24]

161
$$\kappa = \frac{\Delta X}{A \times M_{B2}} \times \frac{2\pi^2 r^4}{(M_{B1}/M_{B2})^2 - 1}$$

162   where, κ is the hydraulic permeability of the porous scaffold, A is the flushing area of the

163   cylindrical scaffold, ΔX is the thickness of the scaffold, M_{B1} and M_{B2} are the mass of the flushed

164   water from outlet in control setup and test setup, respectively.

165   ***D. In-vitro degradation analysis***

166   *In-vitro* degradation of porous AG-CH scaffold was carried out by incubating the samples in

167   sterile PBS solution (pH 7.4) at 37 °C for 4 weeks under non-stirring condition. At weekly

168   intervals, three samples were removed and dried at 60 °C in a hot air oven and then weighed. At

169   the same time, PBS solution was replaced with fresh PBS. The degree of degradation was

170   calculated from the change in dry weight of scaffold.

171          $D_D (\%) = (W_I - W_F)/W_I) \times 100$

172   Where, D_D is degree of degradation, W_I is initial dry weight of incubated sample and W_F is final

173   dry weight of sample after incubation.

174   ***E. Zeta potential analysis***

175   The sample preparation for zeta potential analysis of solids was carried out as per the earlier

176   reported study.[25] In brief, glutaraldehyde-crosslinked AG-CH scaffold was dried (~10 mg dried

177   mass) at 60 °C for 4 h. The scaffold was then ground using mortar-pestle and suspended in 5 mL

178   of ultra pure H_2O. The suspension was sonicated for 1 h at 100 mV and 60% frequency and

179   further analyzed using a Zetasizer analyzer (Nano-Z series, Malvern, UK). Before the analysis,

180 the suspension was dispensed into different vials and pre-assigned pH values (pH 4 to 8) were

181 adjusted with 1 N HCL and 1 N NaOH solutions without addition of background electrolytes.

182 *F. Fourier transform infrared spectroscopy and thermo gravimetric-differential thermal*

183 *analysis*

184 The fourier transform infrared (FT-IR) spectroscopy of native polymers and their composite

185 forms were studied by FT/IR-660 Plus spectrophotometer (Jasco, Japan) at room temperature (27

186 $\pm$ 2). FT-IR samples were prepared in KBr in the ratio of 1:10 (w/w), which were further

187 analysed to understand the chemical attributions before and after polymer crosslinking.

188 Thermogravimetric-differential thermal analysis (TG-DTA) (NETZSCH Thermal analyzer; STA

189 409 pc Luxx, GMBH) of the scaffold was examined from 0 to 700 °C at a heating increment of

190 10 °C.min^{-1} in an inert atmosphere.

191 *G. Rheological characterization*

192 The rheological characterization of AG-CH scaffold was performed on Rheometer- MCR 302

193 (Anton-Paar, Germany) using serrated plates of 8 mm diameter at 37 °C. AG-CH scaffold (8 mm

194 diameter and 3 mm height) was placed between the measuring plates and a gradually increasing

195 force was applied from 1 N to 50 N at a fixed frequency (1Hz) and amplitude (0.1%). The

196 associated software RHEOPLUS was used to record the different variables such as elastic

197 modulus (G'), loss modulus (G") and shear stress (τ).

198 **2.2.3. Hepatocytes compatibility analysis**

199 **A.** *Hepatocyte cell growth in AG-CH scaffold*

200 Hepatocytes were isolated from the liver of an adult male wistar rat (7-8 weeks, 200-215 g) by

201 the liver perfusion method using 0.05% collagenase. The isolated hepatocytes were dispersed in

202   a hormone-defined medium (HDM: Williams medium E supplemented with 10 µg mL^{-1} insulin,

203   0.1 µM CuSO$_4$.5H$_2$O, 3 µg mL^{-1} H$_2$SeO$_3$, 50 pM ZnSO$_4$.7H$_2$O, 50 ng mL^{-1} EGF, 50 µg mL^{-1}

204   linoleic acid, 58.8 µg mL^{-1} penicillin and 100 µg mL^{-1} streptomycin). These cells (cell density;

205   5×10^5 cells mL^{-1}) were seeded drop wise onto medium-equilibrated AG-CH sections (5 mm

206   height and 13 mm diameter) which were pre-sterilized by autoclaving. Cell seeded sections were

207   then cultured in a humidified atmosphere of 5% CO$_2$ and 95% air at 37 °C. The medium was

208   gently replaced after 3h of seeding and routinely after 24 h till end of the experiment. The cell-

209   seeded sections on day 10 were fixed using 2.5% glutaraldehyde solution and then observed

210   under SEM for cell-to-material interaction. Cell-viability was observed by inverted fluorescence

211   microscope (Olympus, Japan) after fluorescien diacetate (FDA) staining. Cell proliferation in

212   AG-CH scaffold was examined every alternate day upto day 10 using MTT assay.[12,26] The

213   relative cell viability (%) was expressed as a percentage relative to the viable cells number.

214   *B. Albumin and Urea assay*

215   For liver specific test, primary rat hepatocyte cells were seeded in the AG-CH scaffolds (5 mm

216   height and 13 mm diameter) placed in wells of 24-well tissue culture plates at a density of 1×10^5

217   cells/well. The medium was changed every other day. At pre-defined time intervals the culture

218   medium was collected and stored at –80 °C for analysis. In the medium, the secreted albumin

219   was measured using enzyme-linked immunosorbent assay (ELISA Albumin Quantification Set;

220   Bethyl, Montgomery, TX) and urea concentrations was determined using Urea assay kit (Sigma-

221   Aldrich, Germany) according to the manufacturer's protocol.

222   *C. Drug detoxification assay*

223   Hepatic cytochrome P450 (CYP450) is a family of enzymes that catalyses the oxidative

224   metabolism of drugs. It is expressed predominantly in the liver tissue and its induction is

225   commonly used for identifying the fate of pharmaceutical residues. The CYP450 activity in the

226   primary hepatocytes seeded into AG-CH scaffold was observed by incubating with freshly

227   prepared 500 µL of ethoxyresorufin (20 µM solution prepared in DMSO) (Sigma-Aldrich,

228   Germany) on day 7. Non-fluorescent ethoxyresorufin metabolized into fluorescence resorufin by

229   viable cells and thus generates fluorescent bright red color signals, which was monitored under

230   fluorescence microscope.

231   **2.2.4. Statistical analysis**

232   For the statistical analysis, samples were studied in triplicate for all the experiments. The

233   obtained experimental values are presented as mean ± standard deviation (SD) for the material

234   characterization. While, the data analysis of cell culture experiments was performed with one-

235   way ANOVA using *Tukey's* honestly significant difference (HSD) test in SPSS software (version

236   10) and differences were considered significant at $P < 0.05$.

237

238   **3. Results and discussion**

239   **3.1. Synthesis of AG-CH scaffold**

240   Agarose and chitosan polymer in the form of composite scaffold was synthesized under

241   moderate freezing condition. At sub-zero temperature, phase separation occurs within the

242   aqueous polymeric system, wherein, water separates from the polymers and forms ice crystals

243   which act as a porogen. Simultaneously, polymer chains present in the unfrozen liquid micro-

244   phase also get crosslinked. After a pre-defined time of incubation, an interconnected and

245   crosslinked porous polymeric network was obtained due to void space formation by melting of

246   the interconnected ice-crystals (porogen). For optimizing the scaffold properties, different ratios

247 of agarose and chitosan were used in the study (Table 1). The optimum concentration of

248 polymers ratio was obtained by setting up various preparations of different concentration of

249 agarose and chitosan for achieving the elasticity and uniform porosity in the scaffold (Table 1).

250 The optimum concentration of agarose to chitosan was found to be 3:1, respectively. In the

251 control set, plain agarose and chitosan formed a 3-D porous scaffold, which was white and

252 yellow in color, respectively.

253 However, the composite AG-CH scaffold was pale yellow in color (Fig. 1A). In the control

254 set, plain agarose and chitosan formed a 3-D porous scaffold, which was white and yellow in

255 color, respectively. However, the composite AG-CH scaffold was pale yellow in color (Fig. 1A).

256 Plain agarose matrix displayed a soft tissue-like elastic property, while chitosan matrix was stiff

257 and brittle in nature. In contrast, optimum concentration of both the polymers (total polymer

258 concentration 4%) provided a suitable elastic property to the composite scaffold (Fig 1B-D).

259 Beside bioactive property of chitosan, it is also suitable for providing stiffness to the scaffold at

260 optimum concentration. In the composite, 1% chitosan was found to be suitable and above this

261 concentration, scaffold displayed brittle nature. On the other hand, agarose provides the soft

262 elastic property to the composite AG-CH scaffold. However, decreasing its concentration

263 resulted in low matrix elasticity, while, increasing the concentration decreased the pore size in

264 the scaffold. Moreover, plain agarose scaffolds showed poor reproducibility (30 ± 10 %)

265 compare to composite AG-CH scaffolds (90 ± 10 %). Thus, 4% composite AG-CH scaffold

266 comprising 3% agarose and 1% chitosan was used for further characterization.

267 **3.2. Morphology and porosity of AG-CH scaffolds**

268 Scanning electron microscope (SEM) was used for determining the porous architecture of

269 scaffolds as well as orientation, randomness and size of pores within the 3D system. The

270   horizontally cross-sectioned SEM images showed non-uniform distribution of pores in both the

271   control scaffolds of agarose and chitosan. Large pore size (upto ∼ 250 μm) and random

272   orientation were observed in agarose scaffolds. Besides, less randomness and small size of pores

273   were seen in chitosan scaffold, however, the average length of pores was short with low surface

274   area (data not shown), which is not appropriate for 3D cell growth. These aspects account for the

275   fragile nature of chitosan scaffold. In contrast, AG-CH scaffold had a porous structure with

276   homogenously distributed pores (Fig. 2A and inset) and showed interconnectivity and were more

277   circular in shape. The pore diameter was found to be in the range of 10 to120 μm, while the

278   majority of pores were lying in between 40-70 μm (Fig. 2B). The distribution of pore wall

279   thickness was in the range of 2 to 5 µm. The results suggest that the average pore diameter of the

280   composite scaffold is large enough to facilitate the migration of mammalian cells.

281   **3.3. Swelling behavior of AG-CH scaffold**

282   A porous system consisting of interconnected pores allows the convective flow of liquid and

283   gaseous exchange. Hence, a water uptake experiment was performed to examine the swelling as

284   well as phase-transition behavior of AG-CH scaffold. The rate of water uptake by AG-CH

285   scaffold with respect to time showed a $\geq 50\%$ increase in weight by capacity within 30 s and it

286   attained equilibrium within 2 min at room temperature (27 °C $\pm$ 2) (Fig. 2C). The swelling ratio

287   of AG-CH scaffold was 15 ± 0.25 (Table 2). Unlike classical hydrogel, a very slight and quick

288   change in dimensions (∼ 1 mm) was monitored during phase-transition from dry to wet. The high

289   and quick water uptake capacity suggests that inter-pore-connections are present in the AG-CH

290   scaffold, which could provide an efficient environment for 3-D cell adhesion and migration.

291   **3.4. Hydraulic permeability of AG-CH scaffold**

292   Growth of cells within the scaffold depends on the efficient supply of nutrient medium which

293   should continuously permeate through the pores. The calculated average hydraulic permeability

294   of the AG-CH scaffold was 4×10^{-4} m^4.N^{-1}.s^{-1} (Table 2), which justifies the ability of macroporous

295   AG-CH scaffold to efficiently permeate liquid through the interconnected pores unlike in the

296   case of hydrogel synthesized at room temperature which contain mesopores. Earlier

297   investigations on the design and characterization of scaffolds have revealed that molecular

298   transport is significantly affected by pore interconnectivity and permeability.[27] Therefore, beside

299   high porosity, the interconnectivity and permeability can be viewed as an important property of

300   the scaffold, which can be readily measured and related to its biological performance like

301   controlled cell growth in a porous scaffold.

302   **3.5. Zeta potential of AG-CH scaffold**

303   The knowledge of electrokinetic charges present on the surface of scaffold could provide a

304   cryptic nature of polymeric matrix which can assist the complex biological process. The electric

305   potential between the interfacial regions near the matrix surface gives a broad idea about the

306   surface chemistry of a material which is defined as its zeta potential or electro-osmotic mobility.

307   Significant variation was observed in the zeta potential (ζ) of AG-CH scaffold at different pH's

308   ranging from 4 to 8 (Fig. 3A). A range of pH was selected because in general, most of the

309   cellular events occur in between this range. The AG-CH scaffold showed a negative zeta

310   potential at neutral pH (-16.3 $\pm$ 0.35 mV), which did not change significantly at pH 8 (-18.0 $\pm$

311   1.4 mV). The point of zero charge (PZC) for AG-CH scaffold was observed at around pH 5.6.

312   Below the PZC, free amine groups (R-NH$_2$) on chitosan are protonated in the ionic form (R-

313   NH$^+_3$) and thus provide positive surface charge to the matrix.[25] The negative zeta potentials

314   above the PZC demonstrated possible surface interaction with OH$^-$ ions. In general,

14

315   hydroxylated polymer surfaces exhibit a net negative charge at neutral pH which serves as a low

316   affinity adhesion receptor by interacting to positively charged cell adhesion proteins that contains

317   either hydrophobic amino acids or positively charged amino acids, namely arginine and lysine.[28]

318   Such interaction are vital in tissue engineering, as it is believed to act in tandem by binding to

319   integrins and may be essential for the maintenance of normal cell phenotypes.[29] Recent studies

320   have also suggested that a net negative surface charge controls cell-to-cell and cell-to-material

321   interaction in the 3-D porous scaffold.[12] Considering the importance of cell-to-cell signaling in

322   hepatocytes, low affinity surface of AG-CH scaffold holds potential as it can provide amiable

323   cell-binding moieties to maintain the stable interaction of cell-to-matrix. Moreover, presence of

324   chitosan which mimics natural GAGs like sequences can elicit biomimetic properties into the

325   scaffold for functional cell growth.

326   **3.6. *In-vitro* degradation of AG-CH scaffold**

327   Rate of degradation of AG-CH scaffold was examined under aseptic conditions in PBS at

328   physiological pH (pH 7.4) and temperature (37 °C ± 1). The degradation was measured in terms

329   of change in dry weight of the scaffold which was periodically recorded. AG-CH scaffold

330   showed 15 ± 0.35 % degradation after four weeks of incubation in PBS. The scaffold showed a

331   gradual degradation rate kinetic as shown in Fig. 3B, which can be attributed to the preferential

332   hydrolytic scission of the hydrophilic polymeric network of agarose and chitosan. In general,

333   long polymer chains (macromolecules) in the scaffold are degraded into small molecules

334   (oligomers) which could disperse into the surrounding aqueous medium.[30] Besides, compact

335   interpenetrating network formed through crosslinking between the polymers can increase its

336   chemical stability compared to non-crosslinked systems.[31]

337   **3.7. FTIR spectroscopy and thermal property of scaffold**

338 The presence of both polymers in the composite scaffold and conformational changes in their

339 functional groups after crosslinking were examined by Fourier transform infrared (FTIR)

340 spectroscopy (Fig. 3C). The spectrum of composite AG-CH scaffold represents a combination of

341 functional groups present in the native polymer chains of agarose and chitosan. The

342 characteristic peaks of 3,6-anhydro-L-galactose skeletal banding was observed at 931, 894 and

343 770 cm^{-1} in composite AG-CH scaffold, which confirms the presence of agarose. A broad band

344 at 3200-3500 cm^{-1} is attributed to the -NH$_2$ and -OH stretching vibrations. The absorption peaks

345 at 1084 cm^{-1} confirms the presence of saccharide structure in composite scaffold.[32] An absorption

346 band at 1672 cm^{-1} is attributed to the formation of C=N bond in the composite scaffold by

347 glutaraldehyde crosslinking.[25] Besides the corresponding characteristic absorption peaks, the

348 symmetric and asymmetric stretching of C-H at 2947 and 2891 cm^{-1} were observed. Peak at *1372*

349 *cm^{-1}* represents the C-O-C stretching of ether.[33] Few other similar peaks were found due to the

350 same functional groups in the polymers and their composite. In addition, broadening of peaks

351 were observed in composite AG-CH suggests the intermolecular complexation between polymer

352 chains.

353 The thermal stability of polymer composite was confirmed by TG-DTA (Fig. 3D). TGA

354 graph showed the first peak drop (~ 3% from initial weight of sample) at 100 °C due to loss of

355 water molecules. The onset of scaffold degradation was observed at 208 °C. Approximately 25%

356 and 50% weight loss was observed at 268 °C and 318 °C, respectively. The lower rate of

357 decomposition is attributed to higher intermolecular bonding between polymers. The DTA graph

358 showed two short exothermic peaks at 268 °C and 594 °C, which is attributed to the possible

359 physical (melting, vaporization and sublimation) and chemical (reduction and break-down)

360 changes in the composite AG-CH scaffold. The solidus temperature of AG-CH scaffold was

361   found to be ~ 200 °C. These results suggest that the scaffold can be autoclaved at 121 °C for

362   sterile clinical applications and is in agreement with an earlier study on chitosan-based

363   scaffold.[13]

364   **3.8. Rheological properties of AG-CH scaffold**

365   The polymeric scaffolds which are often soft materials can deform under applied force, leading

366   to change in the stiffness (storage modulus; G') and fluidity (loss modulus; G") of the scaffold.

367   However, shear stress represents the fracture deformation limit of the material. The results were

368   interpreted from the graph plotted between the storage modulus, loss modulus and shear stress

369   against applied force from 1 N to 50 N at constant frequency (1Hz) and amplitude (0.1%) (Fig.

370   4). In the dry state, storage modulus (G') of AG-CH scaffold was 2×10^6 Pa and did not show any

371   significant change up to 6 N, beyond which a significant change can be seen from the graph (Fig.

372   4A). The dynamic modulus of dried AG-CH scaffold was 6×10^6 Pa. A deformation peak was

373   observed at 27 ± 1 N. The loss modulus (G") of the scaffold showed similar pattern to G' and

374   increasing values of G" can be attributed to the loss of flow (viscous) property of the scaffold by

375   increasing the force. In hydrated condition, a linear increment of G' and G" seen in the graph

376   (Fig. 4B) is suggestive of a resistance in the scaffold against applied force. The elastic modulus

377   of hydrated AG-CH scaffold at 1 N was 1.6×10^5 Pa and dynamic modulus was 1×10^6 Pa, which

378   was significantly less compared to values under dry conditions. Unlike dry, the hydrated AG-CH

379   scaffold did not show any retention time to maintain G' and G", thus it indicates that the scaffold

380   upon hydration loses its stiffness. Additionally, compared to dry scaffold, the hydrated scaffold

381   showed delay in the fracture deformation i.e. 34 ± 1 N, which confirms the higher elastic

382   property of the scaffold in their wet state. More often, non-uniform pore architecture in the

383   scaffold dramatically diminishes the mechanical properties and restricts precise tissue

384 procreation which is a vital concern in 3D cell culture systems.[34] In contrast, a linear increment

385 in the mechanical property of the AG-CH scaffold with respect to increasing force at constant

386 frequency and amplitude provides an understanding of uniform distribution of pores resulting in

387 a higher dynamic modulus (i.e. 1 MPa to 6 MPa) with sponge-like property, indicating that

388 macropores are interconnected in AG-CH without compromising on its mechanical stability and

389 thus holds promise for soft-tissue engineering.

3.9. Hepatocytes compatibility and functionality analysis

391 In order to show that the synthesized AG-CH scaffold has a potential in liver tissue engineering,

392 an initial cell adhesion analysis was performed on AG-CH scaffold using primary hepatocytes.

393 At pre-defined time intervals, hepatocytes behavior in 3-D scaffold was examined by SEM and

394 inverted fluorescence microscope, which showed viability and adherence of hepatocytes on the

395 surface interface of AG-CH scaffold (Fig. 5). After day 10, SEM observations showed

396 distribution of hepatocytes clusters throughout the surface of the AG-CH scaffold, wherein cells

397 were retaining spherical morphology (Fig. 5A), which is a typical behavior of hepatocytes.

398 Moreover, cell secreted extracellular matrix was also become visible after day 10 and delimited

399 the adherence of hepatocytes. Apart from that, the FDA staining validates the viability and

400 clustered cell growth of hepatocytes. These initially *in-vitro* observations suggest that the

401 scaffold was providing a native-like 3D micro-environment to the primary hepatocytes. Wherein,

402 the pores of the scaffold were large enough to allow cells to migrate through the pores with

403 effective delivery of nutrients as well as removal of metabolic waste which are essential for

404 sustaining the cell functionality. The hepatocytes functionality and percent viability in AG-CH

405 scaffold was monitored at periodic time intervals up to day 10 (Fig. 6A). The cell-compatibility

406 of AG-CH scaffold was compared with the control (2D) cell culture (0.1% gelatin-coated

407   polystyrene tissue-culture plates). The calculated relative cell viability was found ~60% after day

408   1, which was decreased to ~40% after day 10 in AG-CH scaffolds and showed less than one-fold

409   decrease. In a control experiment, a significant three-fold decrease in the cell viability from

410   ~45% to ~15% was observed. However, percent cell viability was observed significantly higher

411   in the AG-CH scaffold compared to the control over a period of *in-vitro* cell culture. Unsuitable

412   micro-environmental factors like limited surface area and insignificant cell-surface interaction in

413   the control might be a reason of significant loss in hepatocytes viability.

414   Albumin secretion and urea synthesis by the growing hepatocytes were significantly higher

415   in 3D scaffold compared to control (Fig 6 B,C). In comparison to control, AG-CH scaffolds

416   showed approximate two-fold higher the albumin secretion and approximately three-fold higher

417   the urea synthesis, after day 7. Correlating these liver specific functions with the cell viability

418   suggest the possibility of initial physiological stresses to cells, followed by restoring of ingrown

419   hepatocytes functions by adopting the 3-D microenvironment of AG-CH scaffold, which

420   probably mimicking the liver-like microenvironment. Determination of CYP450 enzymatic

421   activity in mammalian hepatocytes is a most commonly used method for screening of drug

422   compound and detecting general toxicity, where CYP activity can be either induced or inhibited

423   by specific compounds. The CYP450 activity of the seeded hepatocytes was monitored on day 7,

424   by the conversion of ethoxyresorufin to fluorescent resorufin.[35] Since the biocatalytic conversion

425   of ethoxyresorufin occurred inside hepatocytes, temporarily, the increase in fluorescent intensity

426   of developed resorufin was higher within hepatocytes which can diffuse in the surrounding

427   medium over a period of time. Therefore, sample was immediately observed under microscope

428   after incubation. Fig. 7 shows high intensity of resorufin produced inside the cells that is

429   depicting high expression of CYP450 and confers the hepatic functionality of growing

430   hepatocytes. In addition, functional metabolic activity and cell-clusters of the primary

431   hepatocytes were maintained during 3D culture which signifies that the nutrient transport and

432   gaseous exchange in the AG-CH scaffold was quite efficient. These results are in agreement with

433   the very recent study showing effective functionality of primary hepatocytes in a hydrogel made

434   up of de-cellularized liver extracellular matrix (ECM) for liver tissue engineering.[16]

435   Unfortunately, these animal derived ECM for scaffold synthesis have shown limited

436   biocompatibility and immunological concern.[36] Moreover, ECM derived scaffolds are having a

437   major concern of storage and immediate availability for clinical application.

438   Hepatocytes are very unstable and have tendency to lose their cell viability during the in-

439   vitro culture system. However, studies in rat and human hepatocytes have shown that when these

440   cells were cultured under serum-free and hormone-defined medium (similar conditions were

441   used in our study), hepatocytes maintain many markers of differentiation including cellular

442   morphology (round and spheroid), express plasma proteins like albumin, and also activity of

443   metabolic enzymes like CYP450. Functionally, these culture conditions also preserve hepatic

444   stress response pathways.[37] In agreement with these results, our finding show the expression of

445   hepatic biomarker CYP450, maintain round morphology of cells and secret albumin during the

446   in-vitro 3D cell culture in Ag-Ch scaffold. Apart from that, in vitro micro-environment can

447   influence the hepatic stress response which results in delayed functionality of hepatic cells in the

448   3D cell culture. This might be the reason for cells viability decrease irrespective of albumin

449   secretion during the period of cell culture. There are several such reports that explain the similar

450   cellular growth and functional profile of hepatocytes in the in-vitro culture systems.[16,38,39]

451   Additionally, liver ECM not only allows anchorage of hepatocytes but also induce intracellular

452   signaling pathways, thereby enabling sensing of the extracellular milieu with subsequent cellular

453   adaptation to the environment. The complex 3D interaction is believed to be crucial in regulating

454   and maintaining hepatic functions. Therefore, developments in the designing of synthetic

455   scaffolds now offer a range of materials that can culture hepatocytes in 3D. Such artificial ECM

456   as a scaffold for hepatocytes growth is an important key component in liver-like tissue modeling

457   because the interactions of hepatocytes with the optimum artificial ECM and cell–cell contacts

458   are essential in a 3D liver model to maintain hepatocyte polarization and functionality.[40]

459   Considering above parameters, our results are encouraging due to the high hepatocyte binding as

460   well as high cell-cell interaction within interconnected pore network of AG-CH scaffold.

461   In the present study, the ratio of biocompatible and biodegradable natural polysaccharides

462   like agarose and chitosan were optimized at cryo-conditions to achieve soft-tissue like elastic

463   properties in the composite. There are only a few studies that have reported about the synthesis

464   of composite matrices using agarose and chitosan, which were synthesized by different

465   approaches and for different applications. For example, chitosan-agarose microspheres were

466   synthesized by the water-in-oil (w/o) emulsion technique for the delivery of berbamine drug.[41]

467   Similarly, composite chitosan-agarose microgels were synthesized by the microfludic approach

468   and shown for the delivery of anticancer drug i.e. 5-fluorouracil.[42] In general, microfludic

469   approach has the limitation of synthesizing gel with small pores and restriction on synthesis of

470   large-size matrix like monolith scaffold. Also, a recent study has demonstrated synthesis of a

471   conjugated chitosan-agarose hydrogel at room temperature for wound dressing application.[43] In

472   contrast, to the best of our knowledge, this is the first study which has shown the use of

473   optimized concentration of agarose and chitosan to transform it into an elastic and sponge-like

474   scaffold using cryo-polymerization process. The composite scaffold thus synthesized displayed

475   fast hydration capacity due to interconnected pores which were uniformly distributed within the

476   scaffold. Thus, it could quickly uptake the cells when re-hydrated with cell suspension, without

477   using time-consuming and expensive surface modulations with proteins or cell-adhesive peptides

478   as in the case of classical hydrogels. By varying the processing method, the synthesis of spongy-

479   like scaffold with optimum physical and biological properties, as well as with varying shapes

480   (such as monolith, disc or membrane) can be tuned as per the requirement of size of tissue. These

481   scaffolds also overcome the limitations of the classical hydrogels, such as reduced porosity,

482   limited physical stability, poor sponginess, delicate handling due to high fragile nature and off-

483   the-shelf unavailability. Unlike hydrogel, dried AG-CH scaffolds can be stored for years off-the-

484   shelf at room temperature in a sterile environment and then it can be promptly utilized for

485   studying drug metabolism and other liver-specific functions in a stable 3D in-vitro system.

486   **Conclusions**

487   In conclusion, this study demonstrates the novel cryogenic-synthesis of AG-CH composite

488   scaffold for fabricating in-vitro 3D liver tissue models. We could achieve the optimal porosity of

489   40-70 microns with degradability and visco-elasticity properties. Scaffold showed interconnected

490   macropores and biomimetic micro-environment which provides sufficient void volume for the

491   growth and proliferation of primary hepatocytes and displayed liver cells functions under *in-vitro*

492   conditions. These features of scaffold will be valuable for constructing liver-like tissue model for

493   analyzing the new therapeutic agent in the laboratory conditions and also could be optimized for

494   bio-artificial liver development. Overall, results indicate that the sponge-like AG-CH scaffold

495   has a potential in 3D liver tissue engineering. However, *in-vitro* toxicological evaluation of these

496   scaffolds will be the future direction for establishing pre-clinical application.

497

498

503   **Notes and references**

504   **1**   V. Y. Soldatow, E. L. LeCluyse, L. G. Griffith and I. Rusyn, *Toxicol. Res.*, 2013, **2**(1), 23-

505   39.

506   **2**   E. F. A. Brandon, C. D. Raap, I. Meijerman, J. H. Beijnen and J. H. M. Schellens, *Toxicol.*

507   *Appl. Pharm.*, 2003, **189**, 233-246.

508   **3**   S. N. Bhatia, G. H. Underhill, K. S. Zaret and I. J. Fox, *Sci. Transl. Med.*, 2014, **6**, 245sr2.

509   **4**   J. S. Hammond, I. J. Beckingham and K. M. Shakesheff, *Expert Rev. Med. Devices*, 2006,

510   **3**, 21.

511   **5**   S. J. Hollister, Nat. Mater., 4 (2005) 518.

512   **6**   D. Singh, A. Tripathi, S. M. Zo, D. Singh and S. S. Han, *Colloids Surfaces B*, 2014, **116**,

513   502.

514   **7**   E. L. Chaikof, H. Matthew, J. Kohn, A. G. Mikos, G. D. Prestwich and C. M. Yip, *Ann. Ny.*

515   *Acad. Sci.*, 2002, **961**, 96.

516   **8**   S. Levenberg and R. Langer, *Curr. Top. Dev. Biol.*, 2004, **61**, 113.

517   **9**   V. Karageorgiou and D. Kaplan, *Biomaterials*, 2005, **26**, 5474.

518   **10**   E. Sachlos and J. T. Czernuszka, Eur. Cell. Mater., 2003, **5**, 29.

519 **11** A. Kumar and A. Tripathi, in A. Tiwari and R. B. Shrivastava (Eds.), *Biotechnology in*

520   *Biopolymers*, i-Smithers Repra Publication Ltd., UK, (ISBN- 1847355439), 2012, Chapter

521   9.

522 **12** A. Tripathi, T. Vishnoi, D. Singh and A. Kumar, *Macromol. Biosci*., 2013, **13**, 838.

523 **13** N. Kathuria, A. Tripathi, K. K. Kar and A. Kumar, *Acta Biomater.*, 2009, **5**, 406.

524 **14** H. Niiranen, T. Pyhalto, P. Rokkanen, M. Kellomaki and P. Tormala, *J. Biomed. Mater.*

525   *Res. A*, 2004, **69**, 699.

526 **15** A. Tripathi, N. Kathuria and A. Kumar, *J. Biomed. Mater. Res. A*, 2009, **90**, 680.

527 **16** J. S. Lee, J. Shin, H. M. Park, Y. G. Kim, B. G. Kim, J. W. Oh and S. W. Cho,

528   *Biomacromol.*, 2014, **15**, 206.

529 **17** H. Ise, S. Takashima, M. Nagaoka, A. Ferdous and T. Akaike, *Biotechnol. Lett.*, 1999, **21**,

530   209.

531 **18** K. W. Ng, C. C. Wang, R. L. Mauck, T. N. Kelly, N. O. Chahine, K. D. Costa, G. A.

532   Ateshian and C. T. Hung, *J. Orthopaed. Res.*, 2005, **23**, 134.

533 **19** P. D. Benya and J. D. Shaffer, *Cell*, 1982**, 30**, 215.

534 **20** A. Kumar, A. Tripathi and S. Jain, *J. Extra. Corpor. Technol.*, 2011, **43**, 195.

535 **21** D. C. Spray, M. Fujita, J. C. Saez, H. Choi, T. Watanabe, E. Hertzberg, L. C. Rosenberg

536   and L. M. Reid, *J. Cell Biol.*, 1987, **105**, 541.

537 **22** J. Hankiewicz and E. Swierczek, *Clin. Chim. Acta*, 1974, 57, 205.

538 **23** A. Tripathi and A. Kumar, *Macromol. Biosci.*, 2011, **11**, 22.

539 **24** J. Li and A. F. T. Mak, *J. Biomater. Appl.*, 2005, **19**, 253.

540   **25**   C. J. Luk, J. Yip, C. M. Yuen, C. Kan and K. Lam, *J. Fiber Bioeng. Informat.*, 2014, **7**, 35.

541   **26**   T. Mosmann, *J. Immunol. Methods*, 1983, **65**, 55.

542   **27**   J. Fan, X. Jia, Y. Huang, B. M. Fu and Y. Fan, *J. Tissue. Eng. Regen. Med.*, 2013, (in

543   press) (doi: 10.1002/term.1701).

544   **28**   A. D. Cardin and H. J. Weintraub, *Arteriosclerosi*, 1989, **9**, 21.

545   **29**   S. Saunders and M. Bernfield, *J. Cell Biol.*, 1988, **106**, 423.

546   **30**   A. Tripathi, A. B. Hadapad, R. S. Hire, J. S. Melo and S. F. D'Souza, *Enzyme Microb.*

547   *Tech.*, 2013, **53**, 398.

548   **31**   M. Jurga, M. B. Dainiak, A. Sarnowska, A. Jablonska, A. Tripathi, F. M. Plieva, I. N.

549   Savina, L. Strojek, H. Jungvid, A. Kumar, N. Firraz and C. McGuckin, *Biomaterials*, 2011,

550   **32**, 3423.

551   **32**   K. Prasad, G. Mehta, R. Meena and A. K. Siddhanta, *J. appl. Polym. Sci.*, 2006, **102**, 3654.

552   **33**   Y. G. El-Reash, M. Otto, I. M. Kenawy and A. M. Ouf, *Int. J. Biol. Macromol.*, 2011, **49**,

553   513.

554   **34**   C. M. Murphy, M. G. Haugh and F. J. O'Brien, *Biomaterials*, 2010, **31**, 461.

555   **35**   J. Fukuda and K. Nakazawa, Biomicrofluidics, 2011, 5(2), 022205.

556   **36**   U. Boeer, F. F. R. Buettner, M. Klingenberg, G. C. Antonopoulas, H. Meyer, A. Haverich,

557   M. Wilhelmi, *Plos One*, 2014, **9** (8), e105964.

558   **37**   G. K. M. Olsavsky, E. M. Laurenzana and C. J. Omiecinski, *Methods Mol Biol.*, 2010, **640**,

559   115-138.

560   **38**   S. Okada, Y. Kono and K. Shiraki, *Yonago Acta medica* 1999, **42**, 103–112

561   **39**   R. H. Bhogal , J. S. Hodson, D. C. Bartlett, C. J. Weston, S. M. Curbishley, E. Haughton,

562   K. T. Williams, G. M. Reynolds, P. N. Newsome, D. H. Adams and S. C. Afford. *PLoS*

563   *One*, 2011, **6(3)**, e18222. doi: 10.1371/journal.pone.0018222.

564   **40**   P. Godoy, N. J. Hewitt, U. Albrecht, M. E.. Andersen, et al., *Arch Toxicol*, 2013, **87**, 1315–

565   1530.

566   **41**   H. U. Zhang, L. I. Sidong and Y. Lei, *Polímeros (online)*, 2012, **22**, 422.

567   **42**   V. Zamora-Mora, D. Velasco, R. Hernández, C. Mijangos and E. Kumacheva, *Carbohydr.*

568   *Polym.*, 2014, **111**, 348.

569   **43**   S. P. Miguel, M. P. Ribeiro, H. Brancal and P. Coutinho, *I.J. Correia, Carbohyd. Polym.*,

570   2014, **111**, 366.

571

572

573

574

575

576

577

578

579

580

581

582

583

584 **Tables and Figures**

585

586 **Table 1** Optimization of polymers concentration for the synthesis of agarose-chitosan (AG-CH)

587 scaffold*

Concentration of polymers		Property of AG-CH scaffold
AG	CH	
1 %	0.5 %	Gel not formed
	1.0 %	Gel not formed
	1.5 %	Brittle hydrogel
2 %	0.5 %	Weak hydrogel
	1.0 %	Gel with uneven porosity
	1.5 %	Brittle porous gel
3 %	0.5 %	Soft & stable gel
	1.0 %	*Porous, soft-spongy and stable*
	1.5 %	Spongy but brittle
4 %	0.5 %	Spongy but non-elastic
	1.0 %	Porous, spongy & stable
	1.5 %	Porous & brittle
5 %	0.5 %	Decreased non-elasticity & pores
	1.0 %	Increased stiffness & decreased porosity
	1.5 %	Brittle & decreased porosity

588 *Note: All the ratios of polymer were repeated five times.

589

590

591 **Table 2** Physico-chemical properties of AG-CH scaffold

Characteristics of agarose-chitosan (AG-CH) scaffold*	
Porosity (%)	83 ± 2
Average pore diameter range (μm)	40-70
Swelling equilibrium (min)	~ 2
Swelling ratio	15 ± 0.25
Hydraulic permeability ($m^4 N^{-1} s^{-1}$)	4×10^{-4}
Point of zero charge (PZC) at pH	5.6 ± 0.3
Degree of degradation (%) (in four weeks)	15 ± 0.35

592 * All data is represented as average of triplicates with standard deviation (SD).

593

594

595

596

597

598

599

600

601

602

603
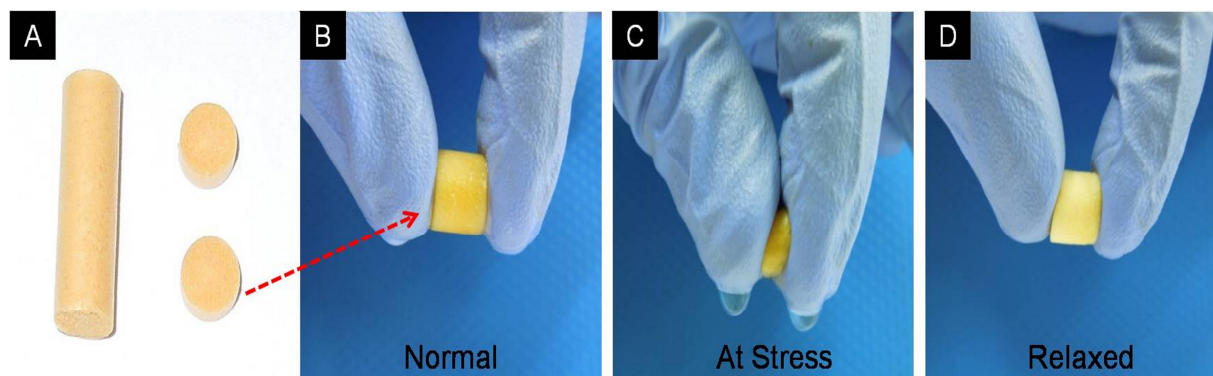
Fig. 1 Composite agarose-chitosan scaffold, (A) can be synthesize in various shapes like monolith and disc format, which shows sponge-like property in series of events; (B) normal (C) at stress and (D) relaxed.

608

609

610

611

612

613

614

615

616

617

618

619

620

621

622

623
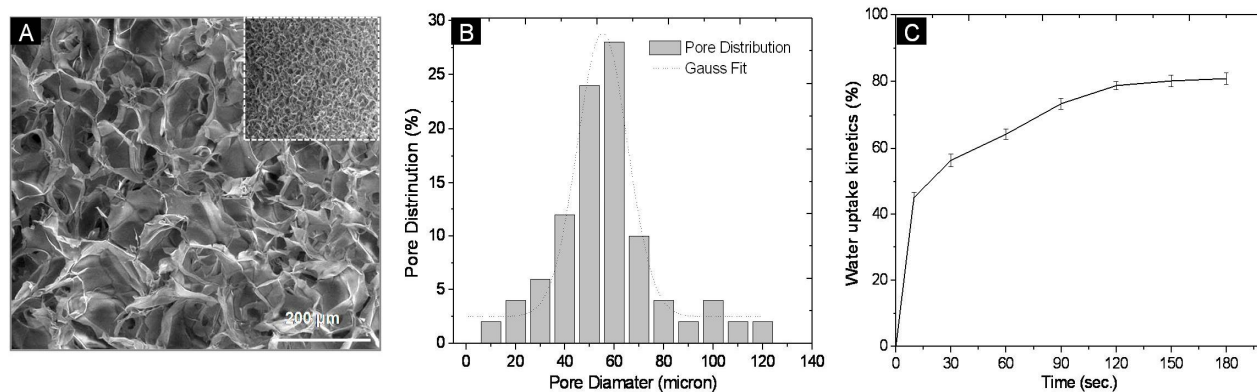
Fig. 2 Morphological characteristics of agarose-chitosan scaffold. (A) scanning electron micrographs shows macroporous morphology and homogenous pore distribution, (B) which is having average pore size range of 40-70 µm and (C) attain its equilibrium within 2 min due to interconnected pore network.

628

629

630

631

632

633

634

635

636

637

638

639

640

641
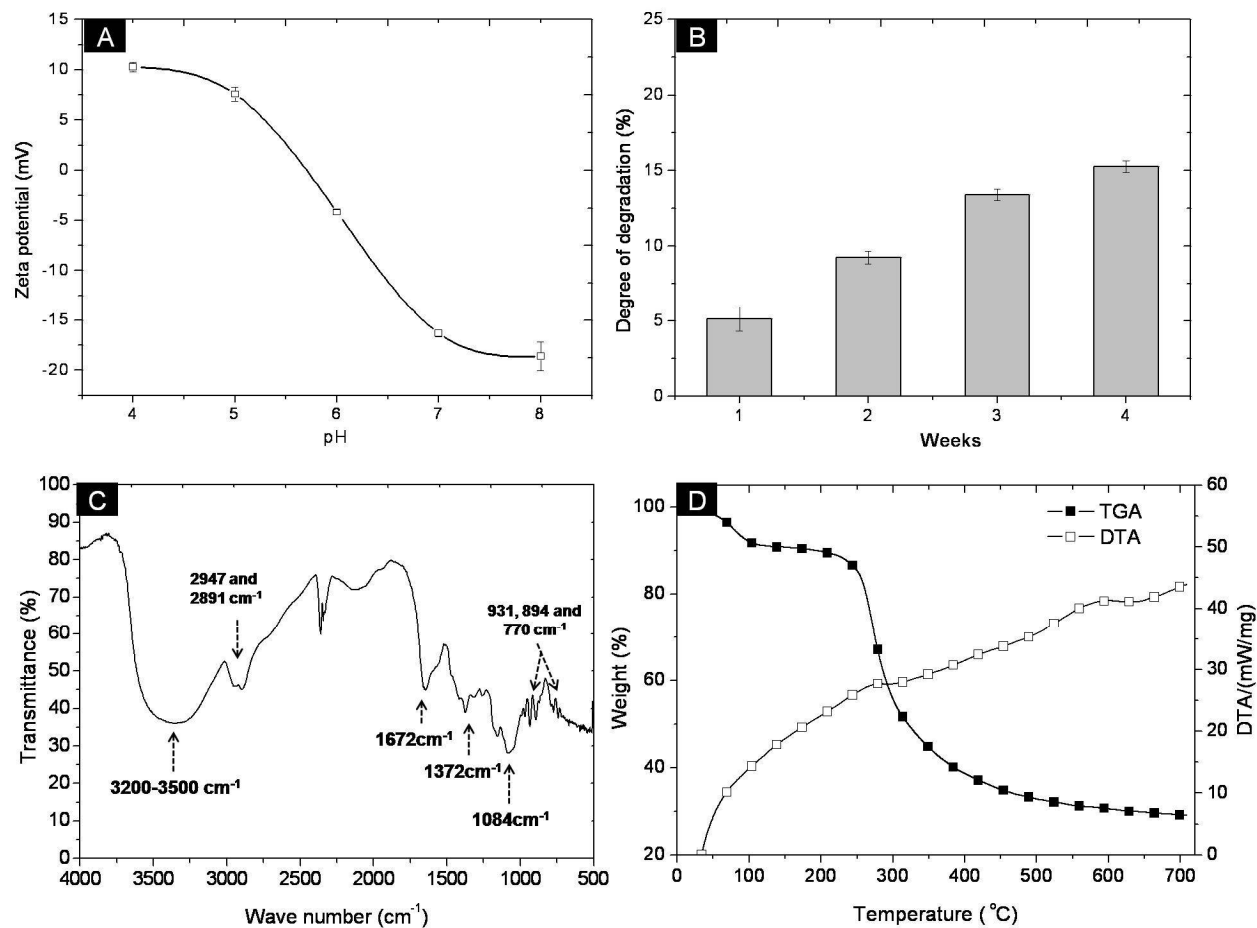
Fig. 3 Characterization of agarose-chitosan scaffold. (A) surface charge analysis by zeta potential, (B) degree of degradation, (C) chemical group attribution by fourier transform infrared spectroscopy and (D) thermal behaviour by TG-DTA analysis.

645

646

647

648

649
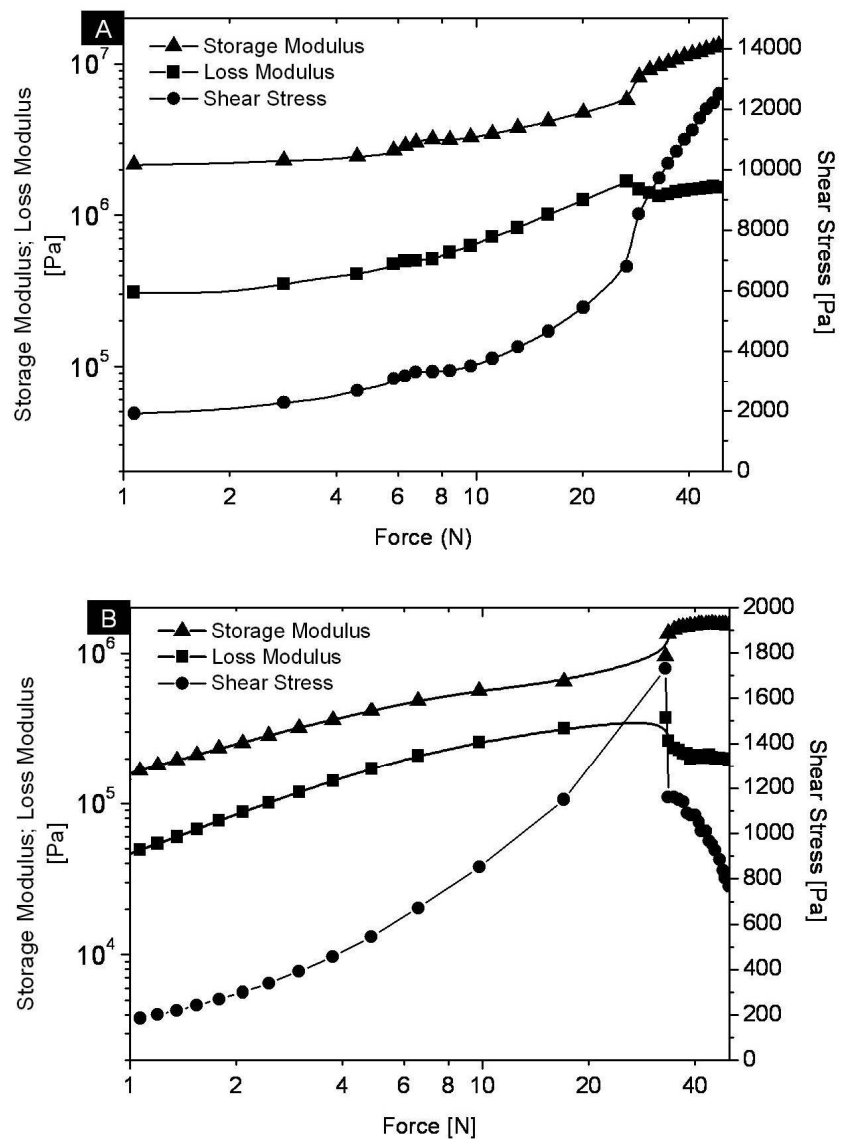
650

651 **Fig. 4** Rheological behaviour of agarose-chitosan scaffold in its (A) dry and (B) wet conditions

652 at 37 °C.

653

654

655

656
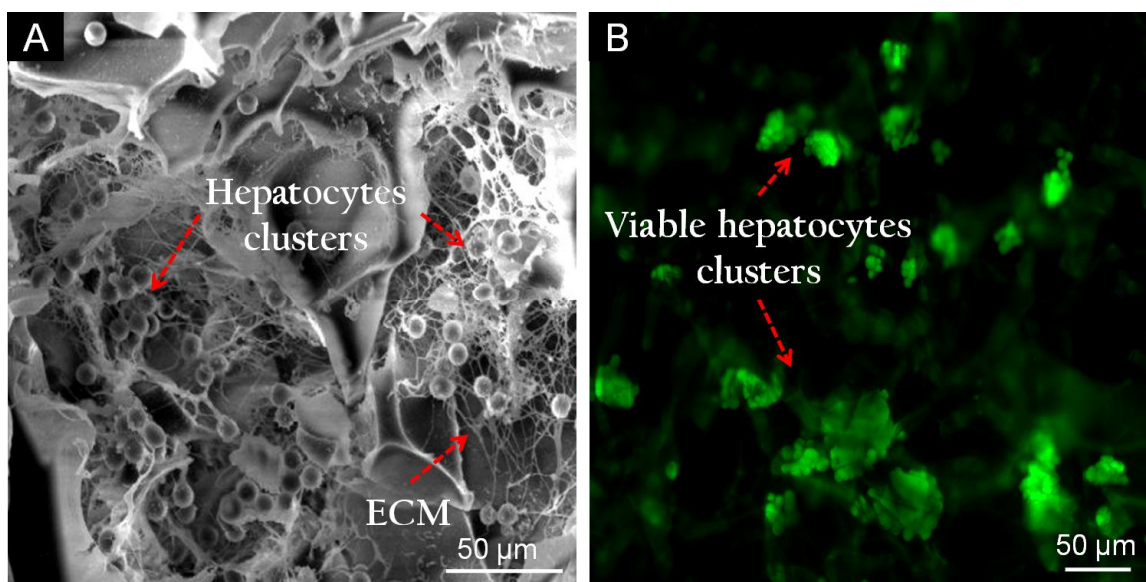
Fig. 5 Hepatocytes on agarose-chitosan scaffold after day 10. (A) SEM micrograph shows cell-to-material interaction, and (B) Fluorescence FDA-staining shows hepatocytes viability.

660

661

662

663

664

665

666

667

668
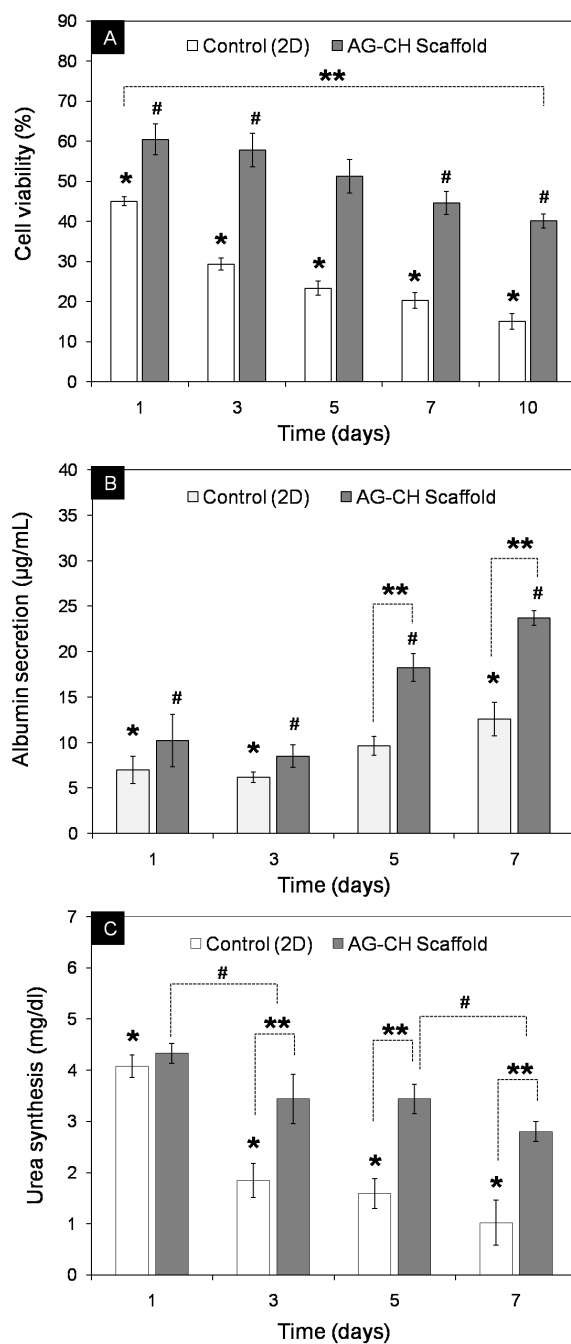
Fig. 6 *In-vitro* quantification of cell functionality. (A) percent cell viability, (B) albumin

secretion and (C) urea synthesis of primary hepatocytes cultured in agarose-chitosan (AG-CH)

scaffold. (*n*=3, *p* < 0.05, * compared to control (2D); # compared to AG-CH scaffold; **

compared 2D and AG-CH scaffold at each data point)

673
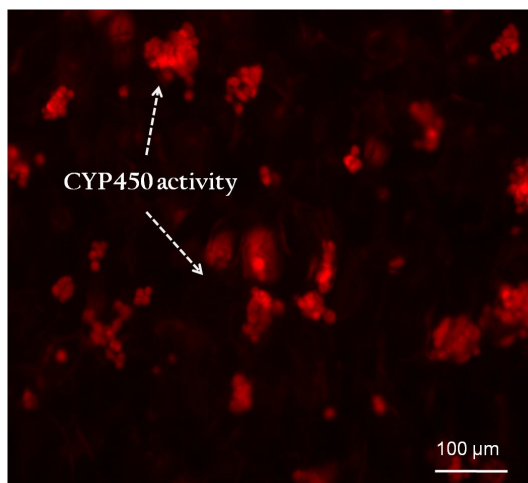
674

675   **Fig. 7** Expression of CYP450 activity of rat primary hepatocytes immobilized in AG-CH

676   scaffold shows fluorescent red resorufin retained in the cell.

677

678

679

680

681

682

683

684

685

686

687 **Graphical Abstract**

688
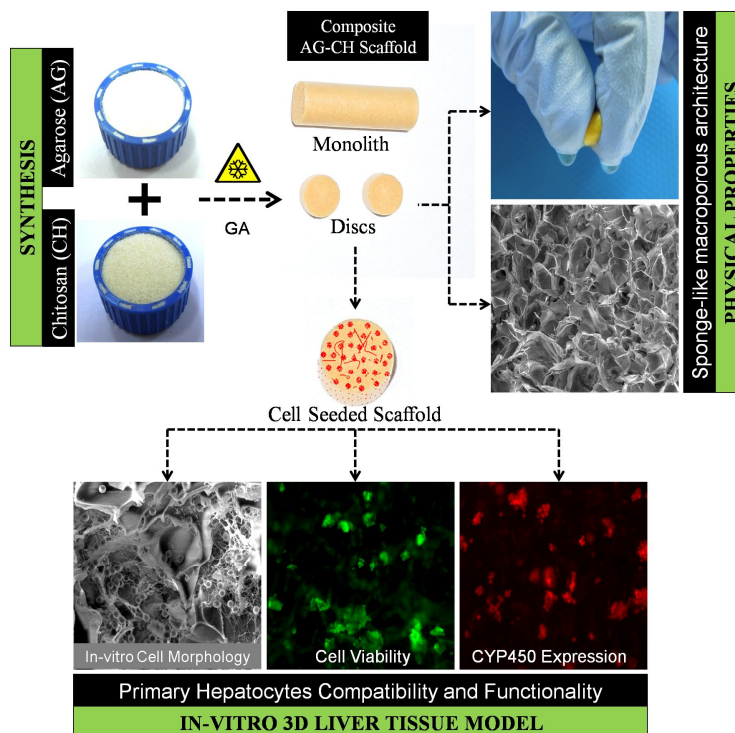
689

690 "Sponge-like agarose-chitosan scaffold synthesized by cryo-polymerization and *in-vitro*

691 evaluation of interfacial cell-material interaction and liver-like functions of impregnate primary

692 hepatocytes"